Available online at www.sciencedirect.com

SciVerse ScienceDirect

Ceramics International 38 (2012) 4835–4844

CERAMICS INTERNATIONAL

www.elsevier.com/locate/ceramint

Influence of Pd-loading on gas sensing characteristics of SnO_2 thick films

L.K. Bagal [a], J.Y. Patil [a], I.S. Mulla [b,c], S.S. Suryavanshi [a,*]

[a] *School of Physical Sciences, Solapur University, Solapur 413255, India*
[b] *National Chemical Laboratory, Pune 411008, India*
[c] *Centre for Materials for Electronic Technology (C-MET), Pune 411008, India*

Received 17 January 2012; received in revised form 22 February 2012; accepted 23 February 2012
Available online 3 March 2012

Abstract

Nanocrystalline pristine and 0.5, 1.5 and 3.0 wt% Pd loaded SnO_2 were synthesized by a facile co-precipitation route. These powders were screen-printed on alumina substrates to form thick films to investigate their gas sensing properties. The crystal structure and morphology of different samples were characterized by using X-ray diffraction, scanning electron microscopy and transmission electron microscopy techniques. The 3.0 wt% Pd:SnO_2 showed response of 85% toward 100 ppm of LPG at operating temperature of 250 °C with fast response (8 s) and quick recovery time (24 s). The high response toward LPG on Pd loading can be attributed to lowering of crystallite size (9 nm) as well as the role of Pd particles in exhibiting spill-over mechanism on the SnO_2 surface. Also selectivity of 3.0 wt% Pd:SnO_2 toward LPG was confirmed by measuring its response to other reducing gases like acetone (CH_3COCH_3), ethanol (C_2H_5OH) and ammonia (NH_3) at optimum operating temperature.

Keywords: SnO_2; Palladium; Thick film; LPG sensor

1. Introduction

For gas sensing applications, three types of solid-state gas sensor are widely used. They are based on solid-state electrolytes, catalytic combustion and semiconductor oxides [1,2]. Metal oxide semiconductor (MOS) based sensors have attracted extensive attention due to their high sensitivity, long-term stability, excellent durability, low production cost, low energy consumption and simplicity in function. MOS gas sensors find numerous applications in: inflammable gas detection, environmental monitoring and security. Among the different MOS materials, tin oxide is known to be a potential material for gas sensor application as its conductivity/receptivity gets tailored in the presence of different oxidizing as well as reducing gases. Near room temperature the oxygen vacancies are frozen and the isothermal changes in conductance of SnO_2 occur due to chemisorptions [3]. A great deal of research efforts has been made to improve the gas-sensing properties of tin oxide sensors. In recent years, the studies on sensor have revealed that the factors influencing gas sensing properties of metal oxides are: grain size of particles [4], microstructure of the sensing body [5] and surface modification of particles (noble metal loading) [6–11].

It is now well accepted that loading of small amount of noble metal, such as Pd and Pt on SnO_2, promotes gas response. In particular, Pd has frequently been loaded on commercial SnO_2-based gas sensors. In this case, sensitization originates by electronic interaction between PdO and SnO_2 as follows; the loading of PdO on SnO_2 increases the electric resistance, because PdO acts as a strong acceptor of electrons and extracts electrons from the oxide. On the other hand, the resistance, when PdO is reduced to Pd on contact with the reducing gases, decreases by back electron transfer from Pd to SnO_2. The difference in electric resistance of SnO_2 induced by a change in oxidized and reduced states of Pd is often large, giving rise to a large increase in response to the reducing gases. It can be proposed that the presence of noble metal catalysts (Pd, Pt, etc.) on the surface of sensing medium enhances response of sensor [12,13]. The catalysts not only create enhanced sites for gas molecular adsorption but also lower activation energy required for the sensing reaction to take place [14,15].

The need for sensors to detect accidental leakage of liquefied petroleum gas (LPG) even at low concentrations has become an acute necessity for both environmental monitoring and human

* Corresponding author. Tel.: +91 217 2744771; fax: +91 217 2744770.
E-mail address: sssuryavanshi@rediffmail.com (S.S. Suryavanshi).

0272-8842/$36.00
doi:10.1016/j.ceramint.2012.02.073

safety perspective, since it creates a serious threat to human lives and personal safety as it is a flammable gas (a mixture of hydrocarbons mainly propane and butane). To afford adequate industry and domestic protection, an effective LPG monitoring system that is simple, reliable, sensitive and cost effective is essential.

The aim of this work is to study the effect of palladium loading on the gas response of SnO_2 thick film. The pristine and Pd-loaded SnO_2 powders were synthesized by co-precipitation method since it is very simple, inexpensive and useful in enhancing the surface area of the material. We have prepared highly sensitive, selective and quickly responding thick films of nanocrystalline pristine SnO_2 and Pd:SnO_2 for LPG sensing using economical screen-printing technique. It is noteworthy that the sensor prepared in this work exhibits better sensing performance in terms of parameters like response and operating temperature as compared to those reported in the literature [16,17].

2. Experimental procedure

2.1. Synthesis of pristine and Pd:SnO_2 nanoparticles and their characterization

The pristine SnO_2 is synthesized by conventional co-precipitation route. An appropriate quantity of stannic chloride ($SnCl_4{\cdot}5H_2O$) and dilute ammonium hydroxide solution (NH_4OH) were used as precursors to form precipitate. The resultant precipitate was then filtered and washed with distilled water for several times to remove chloride ions, which was followed by heat treatment in air at 450 °C for 2 h and the sample was labeled as S1. Thick films were prepared by screen-printing technique as described by Nitta and Haradome [18]. The paste was screen-printed on an alumina substrate (10 mm × 20 mm) by using screen-printing technique.

The Pd:SnO_2 with various wt% Pd were prepared by loading of palladium into pristine SnO_2 nanoparticles with 0.5, 1.5 and 3.0 wt% Pd. The heat treated sample S1 was mixed with 0.5 wt% of the palladium and was labeled as S2, while 1.5 wt% and 3.0 wt% Pd were labeled as S3 and S4, respectively. Similar procedure as described for S1 was utilized to prepare thick films of S2, S3 and S4 samples. Finally all the samples were heat treated at 650 °C for 2 h in air atmosphere. The thermal analysis of the dried precipitate was obtained by thermogravimetric-differential thermal analysis (TG-DTA) performed on SDT Q600 V20.9 Build20 instruments in air with heating rate of 10 °C/min.

The X-ray diffraction (XRD) pattern of the samples was obtained on BRUKER AXS D8-Advanced X-ray diffractometer using Cu-Kα (λ = 1.5418 Å) radiation at 2θ values between 20° and 80°. The surface morphology of all the compositions was obtained using Model JSM-6360 scanning electron microscope instrument. The percentage of constituent elements was evaluated by the energy dispersive X-ray spectroscopy (EDS) technique. The transmission electron microscopic (TEM) analysis and selected area electron diffraction (SAED) were performed on the Philips CM 200 FEG microscope equipped with a field emission gun at an accelerating voltage of 200 kV, with a resolution of 0.24 nm. In order to obtain the high resolution TEM (HRTEM) results we used a Philips Tecnai F 30 107 machine operated at 300 kV. The UV-absorption spectra of pristine SnO_2 and Pd:SnO_2 were performed using JASCO (Model V-670) UV–vis–NIR spectrophotometer. The spectra were taken in the wavelength range of 200–1000 nm for studying the optical band-gap of the samples. FTIR analysis was carried out using a JASCO Model FT/IR-6100 type-A spectrometer in the wave number range of 400–4000 cm^{-1} for studying the chemical groups on the surface of samples S1, S2, S3 and S4 heat treated at 650 °C. The porosity of the films was measured using optical microscope (Carl Zeiss, model-Axiovert 40 MAT and software used is Biovis plus 4.0).

2.2. Gas response measurement

The heat treated screen-printed thick film sensors were tested for gas sensing properties. Digital Nanometer Model DNM-121 and ScienTECH variable power supply ST4074 were used to measure the change in resistance of the sample. Conducting silver paste was used to make ohmic contacts on both ends of thick film and measurements were taken using the gas sensing set-up described earlier [19]. The film was mounted on two probe ceramic sample holder placed in an insulated glass chamber which was inserted coaxially inside a tubular furnace. The area of thick films for all the samples was kept identical and measurements were carried out in air as carrier gas. The gas response measurements were recorded during cooling of the sample after being heated to sufficiently high temperature for stability, thereby securing a good reproducibility of the response temperature characteristics. The resistance of the thick film in air and in presence of test gas was measured as a function of time at different operating temperatures and concentrations of test gas. The responses of all the samples (S1, S2, S3, and S4) were investigated toward liquefied petroleum gas (LPG) at various operating temperatures. The high performance of the sensor was confirmed through the repeatability and reproducibility experiments. For repeatability, two to three cycles of the gas-sensing characteristics were performed on each material. For reproducibility, the gas-sensing performance of at least two to three samples of each type was tested.

The response ($S\%$) to a reducing test gas is defined as:

$$S\% = \frac{R_a - R_g}{R_a} \times 100 \quad (1)$$

where R_a is the resistance of sample in air and R_g is that in the presence of a test gas.

3. Results and discussion

3.1. Characterization of the sensors

Fig. 1 shows the TGA/DTA curves of the dry precipitated powder of S1 to investigate the phase formation temperature. The TGA curve shows three distinct steps of weight loss of the

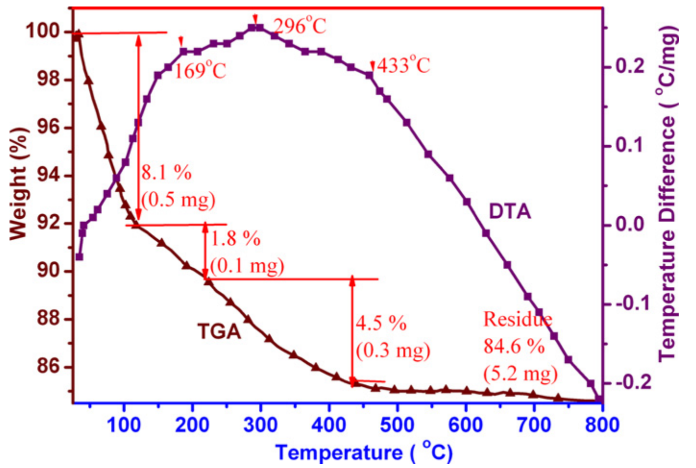

Fig. 1. TGA–DTA profile of the precipitate precursor of pristine SnO_2.

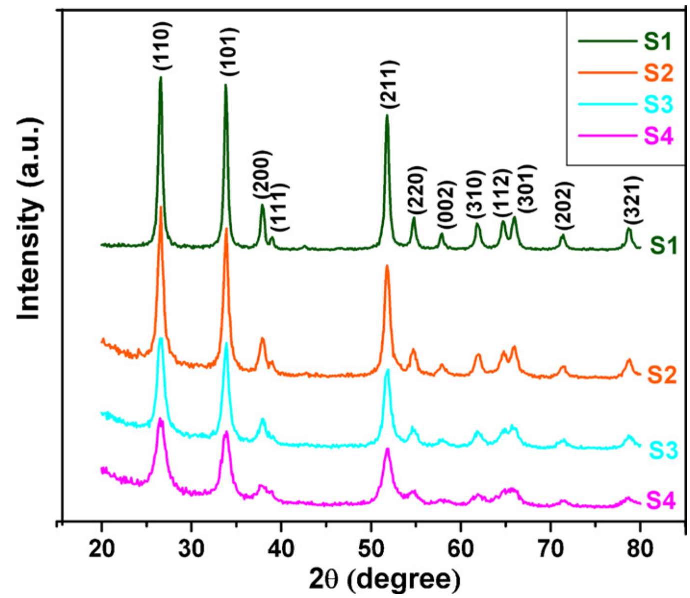

Fig. 2. XRD patterns of (S1) pristine SnO_2, (S2) 0.5 wt%, (S3) 1.5 wt%, and (S4) 3.0 wt% Pd-loaded SnO_2 samples.

powder. In the first step, there is a sharp weight loss up to 8.1% (from room temperature to 125 °C); in the second step there is a weight loss up to 1.8% (125–210 °C) whereas in the third step there is a weight loss up to 4.5% (210–430 °C). The weight loss in the first step is due to the release of the adsorbed water while in other two regions it may be due to crystallization. The desorption of the water appears on DTA curve as an endothermic peak while exothermic peaks on DTA curve around 169 °C and 296 °C represent the decomposition of the residual organic matter. No weight loss is observed after 450 °C implying stable SnO_2 phase formation.

The XRD patterns of heat treated samples of pristine SnO_2 and various wt% of Pd-loaded SnO_2 are shown in Fig. 2. All the

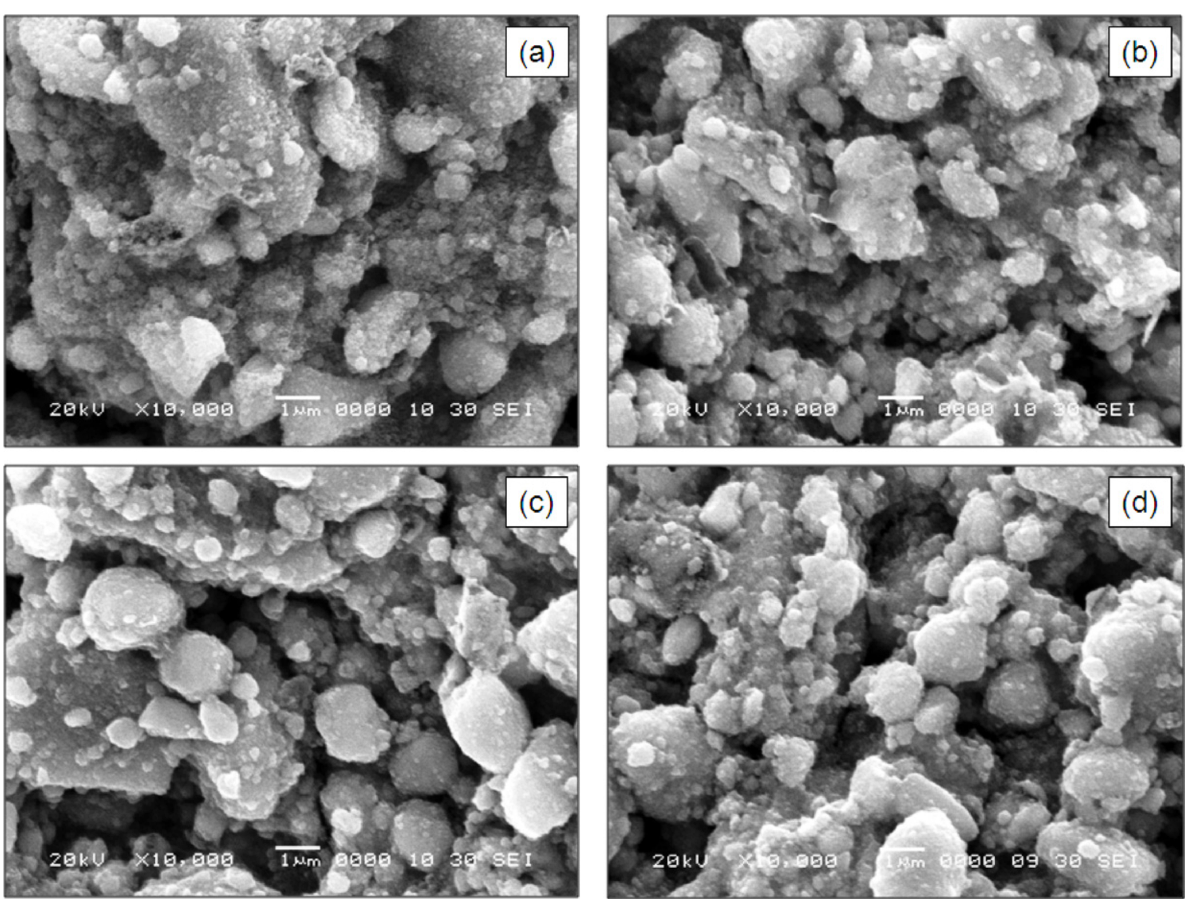

Fig. 3. SEM images of (a) pristine SnO_2, (b) 0.5 wt%, (c) 1.5 wt%, and (d) 3.0 wt% Pd-loaded SnO_2 thick films.

diffraction patterns show characteristic tin oxide peaks with rutile structure [20] without any impurity phase or peaks corresponding to PdO which may be due to concentration of palladium being below the detection level of XRD.

The average crystallite size (D) was estimated using the Scherrer equation as follows:

$$D = \frac{0.9\lambda}{\beta \cos\theta} \quad (2)$$

where λ, β and θ are the X-ray wavelength, the full width at half maximum (FWHM) of the diffraction peak, and the Braggs diffraction angle, respectively.

It is observed that with Pd loading the peaks broaden and relative intensity has reduced, indicating reduction in the crystallite size. The composition with 3.0 wt% Pd:SnO_2 shows lowest crystallite size of around 9 nm, clearly indicating size of materials in the nanometer range. A smaller crystallite size provides a larger surface area for exposure to the test gas, which increases the probability of gas–solid interaction, thereby increasing the response.

Fig. 3 shows the SEM images of heat treated thick films of pristine and Pd-loaded SnO_2 samples. From the micrographs, it is seen that nanocrystalline grains are formed by agglomeration of small particles having irregular shapes and sizes with porous structure.

Table 1
Percentage of porosity and pores/mm^2 of thick films of (S1) pristine SnO_2, (S2) 0.5 wt%, (S3) 1.5 wt%, and (S4) 3.0 wt% Pd-loaded SnO_2.

Sintered thick film samples	Porosity (%) (0–10 μm)	Pores/mm^2
S1	6.4961	176668.3
S2	7.7952	196670.0
S3	8.2338	256519.3
S4	9.9299	453189.3

The porosity of thick films is quantified with the help of optical microscope. Optical image of the sintered samples of pristine SnO_2 and various wt% of Pd-loaded SnO_2 is shown in Fig. 4. The percentage of porosity having pore size up to 10 μm is given in Table 1. This study reveals that as wt% of Pd-loading increases, the porosity increases. The 3 wt% Pd:SnO_2 (S4) film exhibits high porosity as compared to other samples, which seem to contribute for the short response and recovery time. Due to the porous structure diffusion of gas as well as reaction between gas molecules and the interface oxygen species occurs more easily and rapidly. Such porous structure of sample (S4) is desirable for efficient gas sensor applications.

In order to confirm the presence of Pd in SnO_2, EDS analysis was carried out. The EDS spectrum of 3 wt% Pd:SnO_2 (S4) sample is depicted in Fig. 5. The spectrum confirms the presence of palladium, tin and oxygen as per the composition

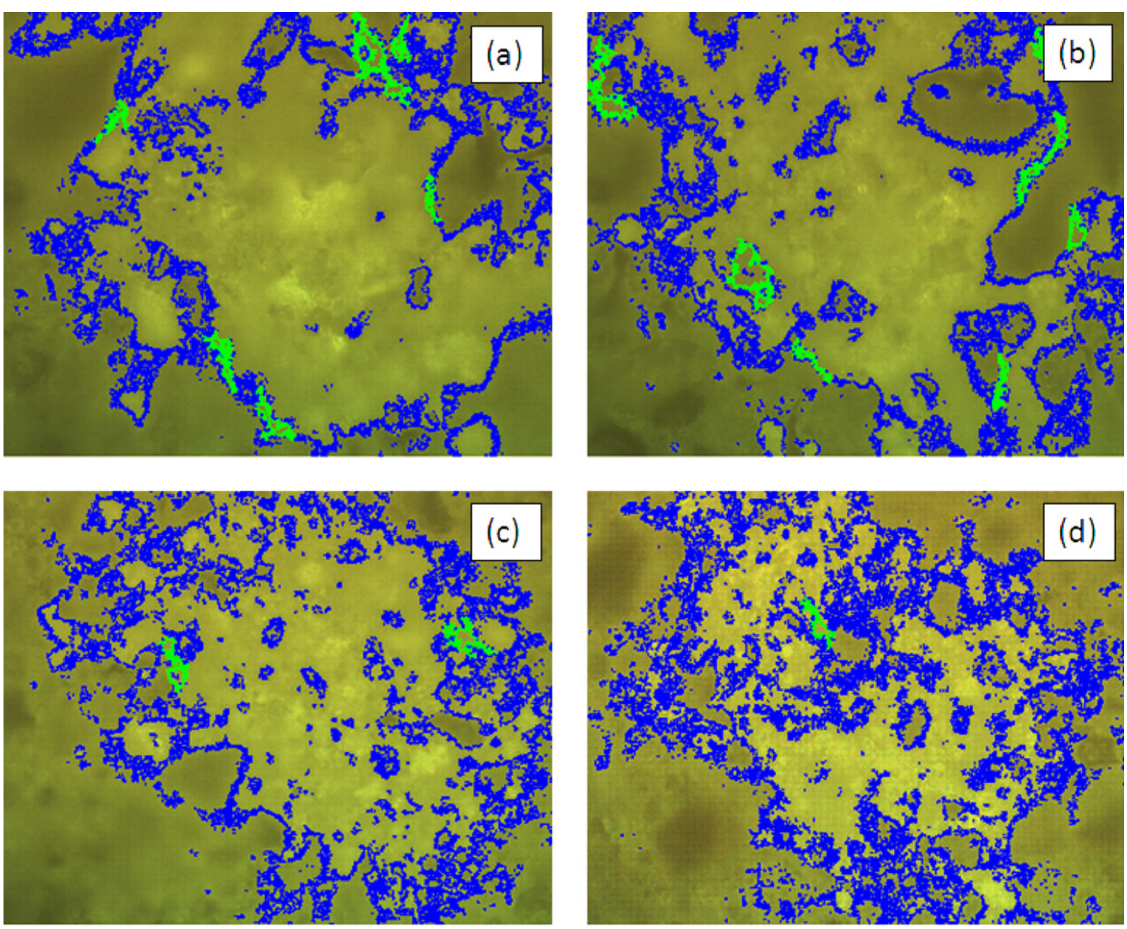

Fig. 4. Optical images of (a) pristine SnO_2, (b) 0.5 wt%, (c) 1.5 wt%, and (d) 3.0 wt% Pd-loaded SnO_2 thick films.

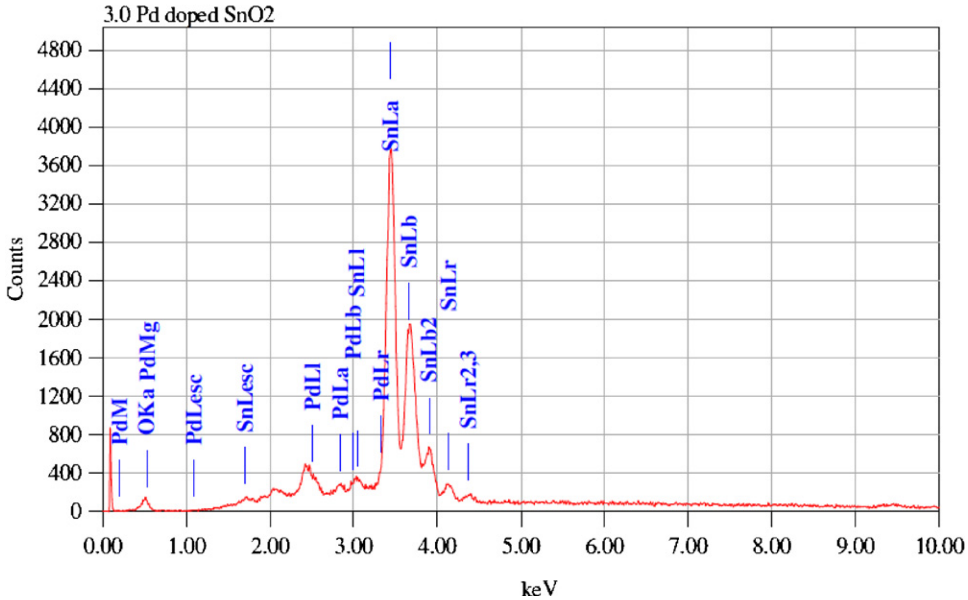

Fig. 5. EDS spectrum of 3 wt% Pd-loaded SnO_2 thick film.

used in the synthesis. Table 2 shows that the EDS data is in good agreement with the initial precursor concentration.

A typical TEM image (Fig. 6(a)) of SnO_2 heat treated at 650 °C, shows formation of nanoparticles around 17 nm sizes. The pristine tin oxide does not show the formation of distinct grains while palladium loaded tin oxide (Fig. 6(b)–(d)) shows distinct grains with size ranging between 5 and 9 nm. It is seen that with loading of Pd the particle size of SnO_2 reduces markedly, which can be attributed to the increase in nucleation sites resulting from higher stacking fault energy due to Pd-loading in the SnO_2

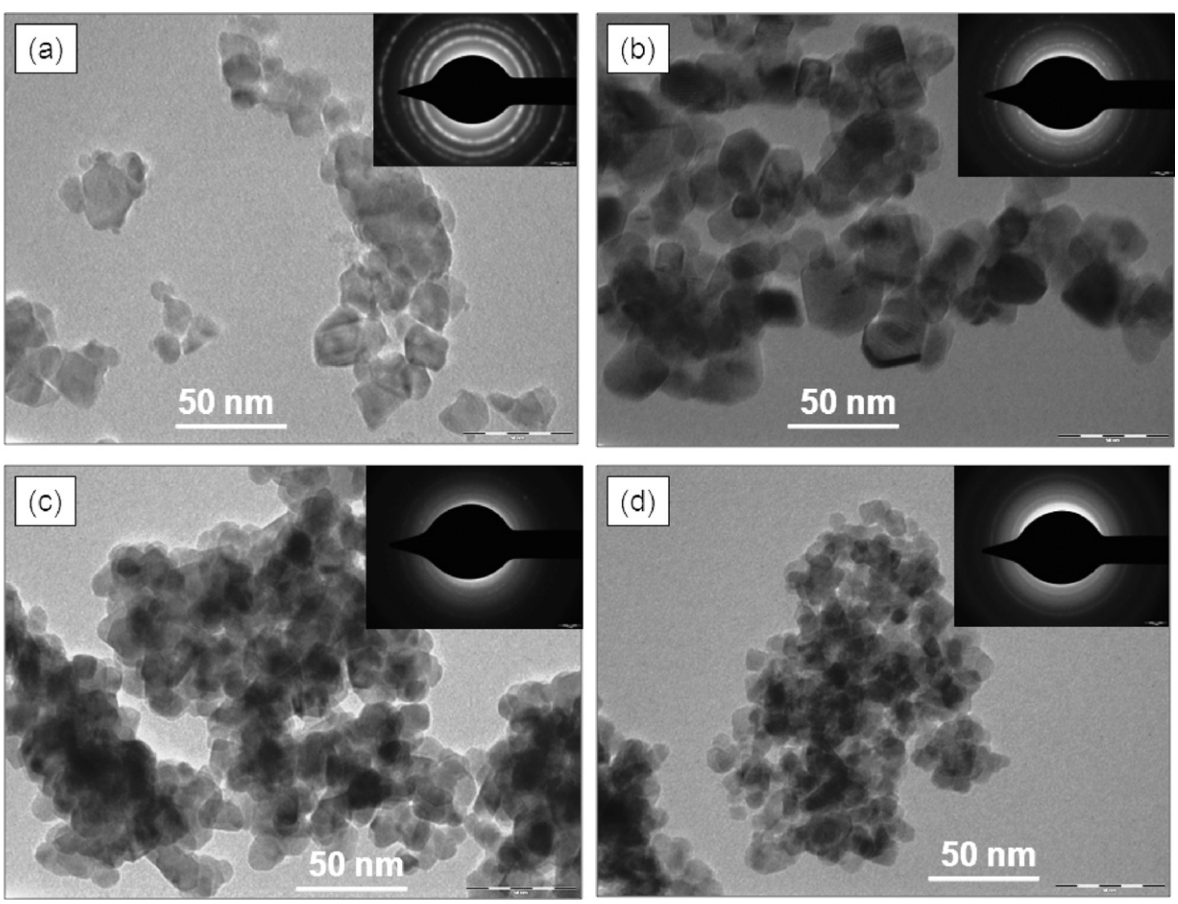

Fig. 6. TEM images with SAED patterns of (a) pristine SnO_2, (b) 0.5 wt%, (c) 1.5 wt%, and (d) 3.0 wt% Pd-loaded SnO_2 samples.

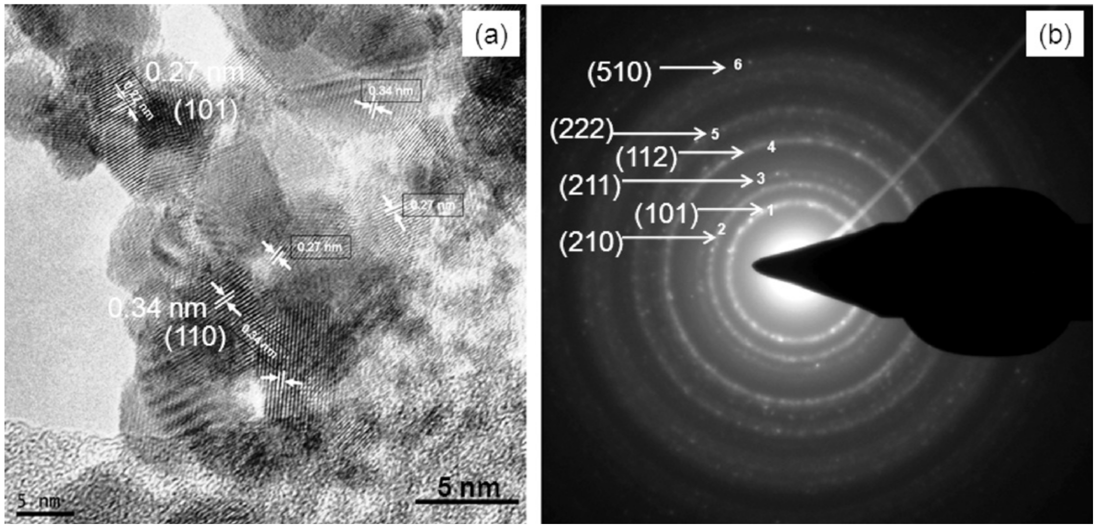

Fig. 7. (a) HRTEM image and (b) SAED pattern of 3 wt% Pd-loaded SnO_2 sample.

material. The selected area electron diffraction (SAED) pattern, shown in inset of an isolated particle exhibits bright rings corresponding to the lattice planes of SnO_2 structure which are in good agreement with the X-ray diffraction pattern. The average particle size which appears from TEM analysis matches well with that calculated by the Scherrer equation from the XRD peaks.

Fig. 7(a) shows the high resolution transmission electron microscopy (HRTEM) image of 3 wt% Pd-loaded SnO_2 particles. This image clearly reveals uniform well crystallized particles. The spacing between the lattice planes along the length and width of nanoparticle was about 0.34 and 0.27 nm which corresponds to (1 1 0) and (1 0 1) planes of the rutile SnO_2, respectively.

The selected area electron diffraction (SAED) pattern (Fig. 7(b)) of an isolated particle shows bright spots corresponding to the (1 0 1), (2 1 0), (2 1 1), (1 1 2), and (2 2 2) lattice planes of rutile SnO_2 structure. These lattice planes match well with the planes observed in the XRD pattern. The structural studies reveal the formation of uniform, distinct nanoparticles of Pd loaded SnO_2, supporting the role of palladium as grain growth inhibitor.

The UV absorption spectra of pristine SnO_2 and Pd:SnO_2 with different Pd concentrations are shown in Fig. 8. Their band gap energy was calculated from their absorption edge. For the direct transition ($n = 1/2$), the optical band gap energy of SnO_2 film was determined by using the equation [21] given below,

$$\alpha = \text{const} \times \frac{(h\nu - E_g)^{1/2}}{h\nu} \quad (3)$$

Table 2
Element concentrations calculated from energy dispersive X-ray spectroscopy (EDS) of 3 wt% Pd-loaded SnO_2.

Element	wt%	at%
O	6.60	34.32
Pd	2.33	1.82
Sn	91.07	63.86

where α is the absorption coefficient, $h\nu$ is the photon energy taken from the UV-spectra and E_g is the optical band gap which was calculated from $(\alpha h\nu)^2$ versus $(h\nu)$ plot. The plot of $(\alpha h\nu)^2$ against $(h\nu)$ is shown in Fig. 8. By extrapolating the linear part of the plot to $\alpha = 0$, the optical band gap of 4.1 eV was estimated for pristine SnO_2, while on increasing the concentration of Pd to 0.5, 1.5, 3.0 wt% the optical band gap systematically reduces to 3.81, 3.71 and 3.59 eV, respectively. This shows that the optical energy band gap decreases with increasing Pd concentration [22]. With increase in Pd concentration, the crystallite size of nanoparticles decreases; the reduction in particle size gives a shift in the optical band gap of the sample. This observation reveals a red shift of band gap energy with addition of Pd relative to pristine SnO_2. The observed shift in band gap values with varying Pd wt% may be attributed to modified phonon spectrum and change in the carrier concentration.

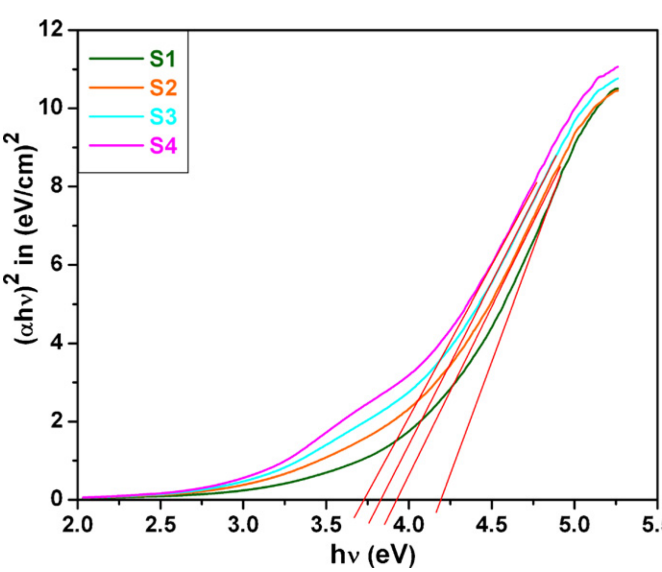

Fig. 8. The influence of Pd-loading on the optical band gap (E_g) from the UV-absorption edge of (S1) pristine SnO_2, (S2) 0.5 wt%, (S3) 1.5 wt%, and (S4) 3.0 wt% Pd-loaded SnO_2 samples.

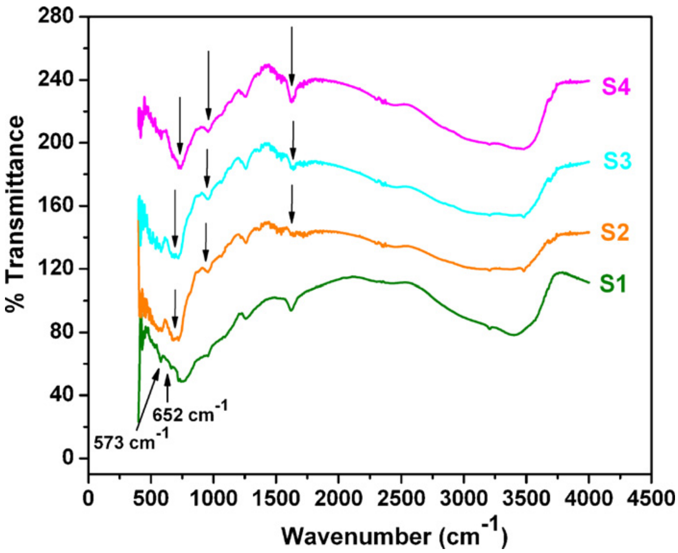

Fig. 9. FTIR spectra of (S1) pristine SnO_2, (S2) 0.5 wt%, (S3) 1.5 wt%, and (S4) 3.0 wt% Pd-loaded SnO_2 samples.

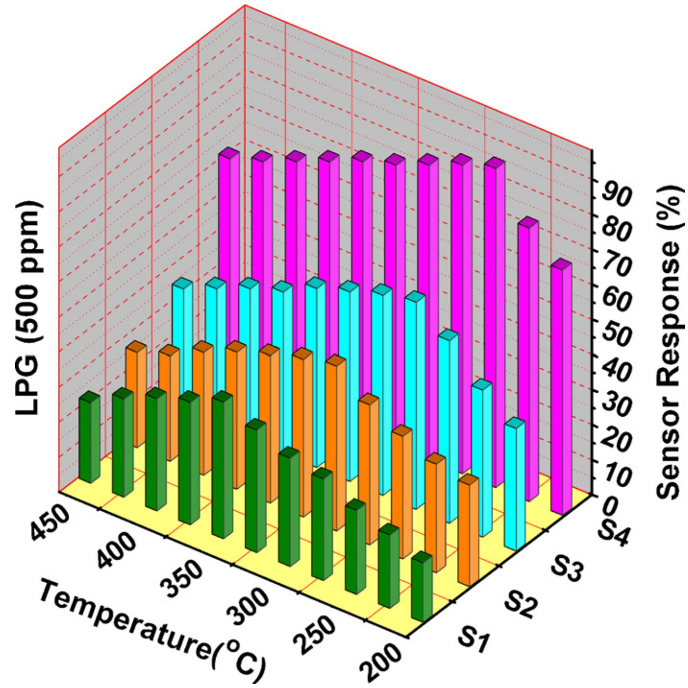

Fig. 10. Correlation between operating temperatures and sensor response of pristine SnO_2 and of various wt% Pd:SnO_2 toward fixed concentration (500 ppm) of LPG.

Fig. 9 shows the FTIR spectra for studying the chemical groups on the surface of the heat treated samples S1, S2, S3, and S4. The bands around 573 and 652 cm^{-1} can be attributed to the Sn–O stretching vibration and the O–Sn–O bending vibration in SnO_2. The bands around 3400 and 1615 cm^{-1} are due to the O–H vibrating mode of the absorbed water [23], while the band located at 1258 cm^{-1} is owing to the bending vibration of –CH_2, which is due to absorption of few organic groups on the surface of SnO_2 nanoparticles [24]. The change in intensity around 1615 cm^{-1} in FTIR-spectra of samples S2, S3 and S4 is proposed to be induced by free electrons in the conduction band as Pd concentration increases.

3.2. Gas sensing properties

The LPG response of samples S1, S2, S3 and S4 is depicted in Fig. 10 as a function of operating temperature toward 500 ppm concentration of LPG. Each sensor exhibits highest response to LPG at its optimal temperature. The S4 shows maximum response of 91% at 250 °C, which is the highest among other samples S1 (39% at 350 °C), S2 (47% at 300 °C), S3 (59% at 275 °C) which can be attributed to smaller particle size exhibited by the S4. It is observed that Pd promotes the gas response (*S*%) and shifts the maximum response toward lower temperatures. The presence of Pd species leads to the formation of surface states just below the conduction band of tin oxide. At higher temperatures oxygen is adsorbed on the sensor surface by capturing electrons from the conduction band. When a reducing gas comes in contact with the sensor, it undergoes oxidation by reacting with adsorbed oxygen. Thus, palladium oxide promotes the sensing activity leading to an enhancement in response as compared with pristine tin oxide. The change in the porosity and distribution of the Pd species is responsible for enhancing the response of the thick films at lower operating temperature.

The maximum response of 3 wt% Pd:SnO_2 sensor to LPG is probably due to smaller grain size which provides a large specific surface area and a higher surface activity, which result in stronger interaction between LPG molecules and the surface adsorbed oxygen species [25]. Palladium acts as a catalyst and enhances the reaction rate, especially because $\chi O - \chi Pd < \chi O - \chi Sn$ where χ represents electronegativity value (χO, χPd, χSn = 3.5, 2.2, 1.9, respectively) [26]. Atoms with a higher electronegativity (close to oxygen (Pd)) induce an electronic transfer from the oxide surface to the metal deposit. In this case, an interaction between the deposited metal atoms and the cations of the surface seems to determine the electronic transfer.

The manifestation of the maximum response at optimal operating temperature is also associated with the formation of charged oxygen ions on the oxide surface. It is possible that Pd-loading not only decreases the particle size but also increases the catalytic activities of the sensor. One of the probable explanations for shift in optimal operating temperature toward lower temperature is due to the reduction in the particle size with Pd-loading concentration.

To confirm the selectivity of S4 toward LPG, the response of the S4 material to other reducing gases like acetone (CH_3COCH_3), ethanol (C_2H_5OH) and ammonia (NH_3) was also measured at optimum operating temperature. Fig. 11 depicts the gas sensing properties of S1, S2, S3, and S4 toward different test gases at 250 °C for 100 ppm concentration. All the samples are highly selective toward LPG as compared to the other test gases. However, with 3 wt% Pd:SnO_2 the selectivity toward LPG improves markedly and its response is about fivefold of the S1 sensor. The S4 sample has proved to be the

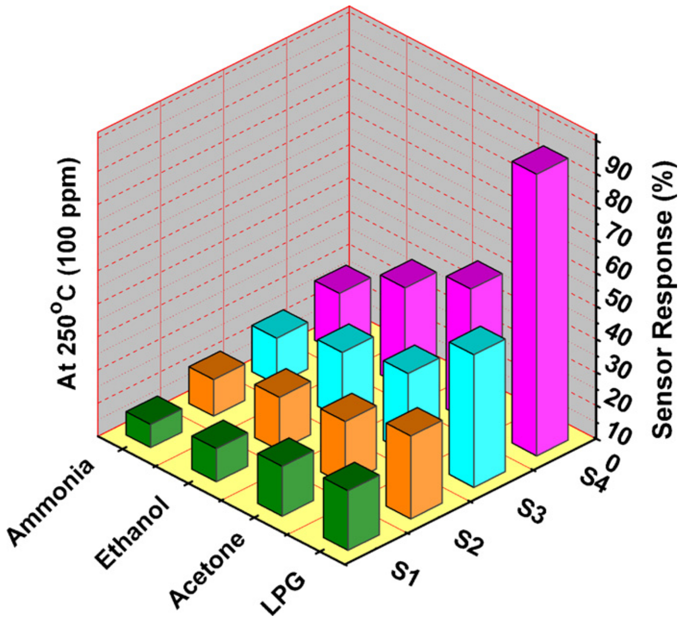

Fig. 11. Selective histogram of pristine SnO_2 and of various wt% Pd:SnO_2 at 250 °C toward 100 ppm concentration of different gases.

potential candidate for LPG detection at relatively lower operating temperature.

It is well known that LPG consists of CH_4, C_3H_8, C_4H_{10}, etc., and in these molecules the reducing hydrogen species are bound to the carbon atoms. When the sensor is exposed to LPG, the hydrocarbons namely propane (C_3H_8), and butane (C_4H_{10}) present in LPG interact with the adsorbed oxygen ions present on the surface of the sensor. The hydrocarbons are converted to CO_2 and H_2O due to their interaction with the adsorbed oxygen ions. The overall reaction of LPG molecules with adsorbed oxygen species can be explained based on the following reactions [27]:

$$O_{2(ads)} + e^- \rightarrow O_2{}^-{}_{(ads)} \tag{4}$$

$$O_2{}^-{}_{(ads)} + e^- \rightarrow 2O^-{}_{(ads)} \tag{5}$$

$$C_nH_{2n+2} + 2O^-{}_{(ads)} \rightarrow H_2O + C_nH_{2n}{:}\ O + e^- \tag{6}$$

$$C_nH_{2n}{:}\ O + O^-{}_{(ads)} \rightarrow CO_2 + H_2O + e^- \tag{7}$$

where C_nH_{2n+2} denotes C_3H_8, C_4H_{10}, etc. and C_nH_{2n}:O represents partially oxidized intermediates on the SnO_2 surface. This reaction produces CO_2 and H_2O and releases the trapped electrons back to the conduction band of the sensing material, leading to an increase in conductance (a decrease in potential barrier). As a result the resistance of the sensing material decreases upon exposure to LPG.

In case of Pd, chemical sensitization plays a significant role in improving the resistance change and so the response of the sensor [28–30]. Pd being a better oxygen dissociation catalyst than SnO_2 enhances the rate of dissociation and diffusion of oxygen species on the surface of SnO_2. The resulting dissociative adsorption of oxygen on the surface results in a greater degree of electron withdrawal from the conduction band of SnO_2. This mechanism is known as the ''spill-over'' effect [28]. The oxidation state of Pd changes when it is in intimate contact with sensing gas molecule due to electron exchange from Pd to oxygen, which produces a change in the resistivity of the sensor.

Pd is known to form metallic clusters on the surface of tin oxide grains, creating additional adsorption sites and catalyzes the surface redox reaction with reducing gases. When a reducing gas is oxidized on the sensor surface, the PdO is converted to Pd, which leads to disappearance of the electronic interactions between the noble metal and the semiconductor.

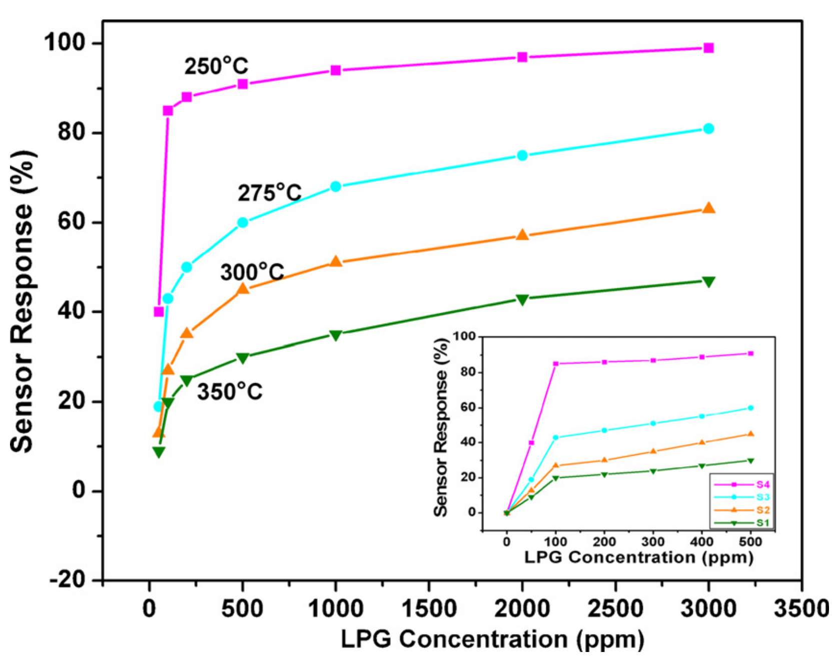

Fig. 12. Sensor response of pristine SnO_2 and of various wt% Pd:SnO_2 as a function of LPG concentration at the optimal operating temperatures.

This change in oxidation state is contributed to the high response of the sensor. The enhanced response of the Pd-loaded SnO_2 film can be attributed to the formation of highly reactive species according to the reaction [31],

$$O_2 + Pd_2 \rightarrow 2Pd : O \tag{8}$$

The Pd atoms are weakly bonded with the oxygen gas, and the resulting complex is readily dissociated at relatively low temperature producing the oxygen atoms. Thus, these oxygen atoms capture electrons from the surface layer and acceptor surface states are formed. The reducing gas reacts with surface adsorbed oxygen decreasing the resistance of sensor material.

The change in gas response as a function of concentration of LPG for all the samples of SnO_2 at their optimal operating temperature is shown in Fig. 12. From the plot, it is quite clear that the sensor response gradually increases up to 1000 ppm of LPG concentration and is saturated beyond 1000 ppm. At a low concentration of gas, when exposed on a fixed surface area of a sample, there is a lower coverage of gas molecules on the surface and hence lower surface reaction occurs. An increase in gas concentration increases the surface reaction due to a larger surface coverage. A further increase in surface reaction will be gradual when the saturation point on the coverage of molecules is reached.

The transient response characteristics of all the samples at 100 ppm LPG concentration are shown in Fig. 13. In these measurements, gas was introduced into the glass tube and sensor's resistivity was measured in air and in the presence of LPG. Fast response (8 s) was observed in the case of sample S4, which may be attributed to the presence of Pd, which catalyzes the reaction promoting the rapid electron transfer between the adsorbate and the adsorbent. The sensor response rejuvenate to its initial value after purging the LPG away which indicates the surface of SnO_2 regains the original microstructure after refreshing with carrier gas (air). The faster recovery (24 s) may be due to the high reactivity of LPG with adsorbed oxygen in the presence of Pd sites on the surface of the sensor. The faster response and recovery would also be attributed to the highly porous nature of the film.

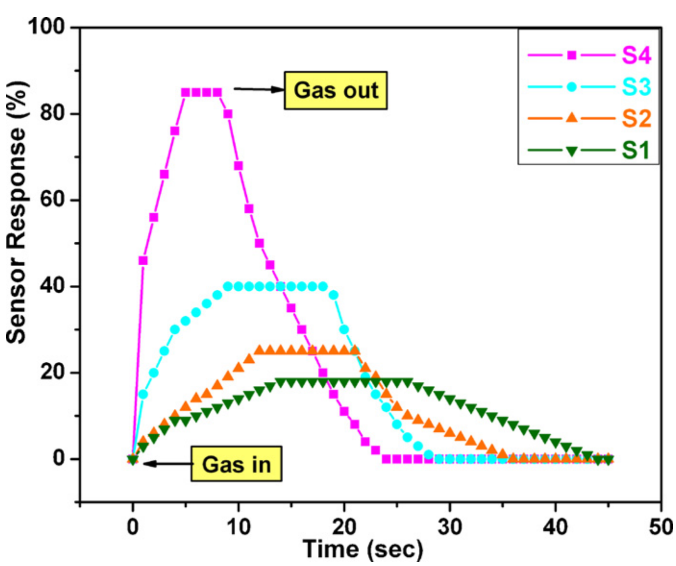

Fig. 13. Transient response characteristics of pristine SnO_2 and of various wt% Pd:SnO_2 exposed to 100 ppm LPG at 250 °C operating temperatures.

4. Conclusions

We have successfully developed nanostructured pristine SnO_2 and Pd-loaded SnO_2 thick film sensors. The loading of palladium found to affect significantly the gas response and morphological properties of SnO_2 due to reduction in the grain size. The sensor S4 (3 wt% Pd in SnO_2) exhibited high selectivity and response of 85% toward 100 ppm of LPG at relatively low temperature. The response is fivefold as compared to that observed for pristine SnO_2. Our results reveal that 3 wt% Pd loaded SnO_2 has remarkable sensing characteristics proving to be a promising material for LPG detection in practical applications.

Acknowledgements

One of the authors, Latika K. Bagal would like to thank the University Grants Commission (UGC) for providing teacher fellowship under FIP and Dr. K.N. Ganage, Principal, K.B.P.M. Pandharpur. J.Y. Patil acknowledges DAE-BRNS for the grant of JRF. I.S. Mulla is grateful to CSIR, New Delhi, India, for granting Emeritus Scientist Scheme. All the authors gratefully acknowledge DAE-BRNS, India, for the financial support. Authors kindly acknowledge the SAIF – IIT Bombay for providing the TEM facility.

References

[1] N. Yamazoe, Toward innovations of gas sensor technology, Sens. Actuators B: Chem. 108 (2005) 2–14.

[2] C.R. Yonzon, D.A. Stuart, X. Zhang, A.D. McFarland, C.L. Haynes, R.P. Van Duyne, Towards advanced chemical and biological nanosensors – an overview, Talanta 67 (2005) 438–448.

[3] S. Munnix, M. Schmeits, Electronic structure of tin dioxide surfaces, Phys. Rev. B 27 (1983) 7624–7635.

[4] C. Xu, J. Tamaki, N. Miura, N. Yamazoe, Grain size effects on gas sensitivity of porous SnO_2-based elements, Sens. Actuators B: Chem. 3 (1991) 147–155.

[5] K. Yoshida, K. Shimanoe, N. Yamazoe, Preparation of SnO_2 cluster by hydrothermal treatment for highly sensitive thin film sensor, in: Proceedings of the Technical Digest of the 6th East Asian Conference on Chemical Sensor, 2005, pp. 515–516.

[6] N. Yamazoe, Y. Kurokawa, T. Seiyama, Effects of additives on semiconductor gas sensors, Sens. Actuators 4 (1983) 283–289.

[7] S. Matsushima, T. Maekawa, J. Tamaki, N. Miura, N. Yamazoe, Role of additives on alcohol sensing by semiconductor gas sensor, Chem. Lett. (1989) 845–848.

[8] T. Maekawa, J. Tamaki, N. Miura, N. Yamazoe, Sensing behavior of CuO-loaded SnO_2 element for H_2S detection, Chem. Lett. (1991) 575–578.

[9] J.G. Duh, J.W. Jou, Catalytic and gas sensing characteristics in Pd-doped SnO_2, J. Electrochem. Soc. 136 (1989) 2740–2747.

[10] J. Kappler, N. Barsan, U. Weimar, A. Dieguez, J.L. Alay, A. Romano-Rodriguez, J.R. Morante, W. Gopel, Correlation between XPS, Raman and TEM measurements and the gas sensitivity of Pt and Pd doped SnO_2 based gas sensors, Fresen. J. Anal. Chem. 361 (1998) 110–114.

[11] K.H. Cha, H.C. Park, K.H. Kim, Effect of palladium doping and film thickness on the H_2 gas sensing characteristics of SnO_2, Sens. Actuators B: Chem. 21 (1994) 91–96.

[12] S.J. Ippolito, S. Kandasamy, K. Kalantar-zadeh, W. Wlodarski, Hydrogen sensing characteristics of WO_3 thin film conductometric sensors activated by Pt and Au catalysts, Sens. Actuators B: Chem. 108 (2005) 154–158.
[13] A. Kolmakov, D.O. Klenov, Y. Lilach, S. Stemmer, M. Moskovitst, Enhanced gas sensing by individual SnO_2 nanowires and nanobelts functionalized with Pd catalyst particles, Nano Lett. 5 (2005) 667–673.
[14] Y. Shen, T. Yamazaki, Z. Liu, D. Meng, T. Kikuta, Hydrogen sensing properties of Pd-doped SnO_2 sputtered films with columnar nanostructures, Thin Solid Films 517 (2009) 6119–6123.
[15] Y.I. Lee, K.J. Lee, D.H. Lee, Y.K. Jeong, H.S. Lee, Y.H. Choa, Preparation and gas sensitivity of SnO_2 nanopowder homogenously doped with Pt nanoparticles, Curr. Appl. Phys. 9 (2009) S79–S81.
[16] J.K. Srivastava, P. Pandey, V.N. Mishra, R. Dwivedi, Sensing mechanism of Pd-doped SnO_2 sensor for LPG detection, Solid State Sci. 11 (2009) 1602–1605.
[17] S. Gupta, R.K. Roy, M. PalChowdhury, A.K. Pal, Synthesis of SnO_2/Pd composite films by PVD route for a liquid petroleum gas sensor, Vacuum 75 (2004) 111–119.
[18] M. Nitta, M. Haradome, Thick-film CO gas sensor, IEEE Trans. Electron Devices ED-26 (1979) 247–249.
[19] R.C. Pawar, J.S. Shaikh, A.V. Moholkar, S.M. Pawar, J.H. Kim, J.Y. Patil, S.S. Suryavanshi, P.S. Patil, Surfactant assisted low temperature synthesis of nanocrystalline ZnO and its gas sensing properties, Sens. Actuators B 151 (2010) 212–218.
[20] N.S. Ramgir, I.S. Mulla, K.P. Vijayamohanan, A room temperature nitric oxide sensor actualized from Ru-doped SnO_2 nanowires, Sens. Actuators B 107 (2005) 708–715.
[21] X. Zhang, X.M. Li Chen, J.M. Bian, C.Y. Zhang, Structural and optical properties of $Zn_{1-x}Mg_xO$ thin films deposited by ultrasonic spray pyrolysis, Thin Solid Films 492 (2005) 248–252.
[22] M. Boshta, F.A. Mahmoud, M.H. Sayed, Characterization of sprayed SnO_2:Pd thin films for gas sensing applications, J. Ovonic Res. 6 (April (2)) (2010) 93–98.
[23] C.P. Sibu, S.R. Kumar, P. Mukundan, K.G.K. Warrier, Structural modifications and associated properties of lanthanum oxide doped sol–gel nanosized titanium oxide, Chem. Mater. 14 (2002) 2876–2881.
[24] D.L. Chen, L. Gao, Novel synthesis of well-dispersed crystalline SnO_2 nanoparticles by water-in-oil microemulsion-assisted hydrothermal process, J. Colloid Interface Sci. 279 (2004) 137–142.
[25] X. Niu, H. Zhong, X. Wang, K. Jiang, Sensing properties of rare earth oxide doped In_2O_3 by a sol–gel method, Sens. Actuators B 115 (2006) 434–438.
[26] V.A. Chaudhary, I.S. Mulla, K. Vijayamohanan, Selective hydrogen sensing properties of surface functionalized tin oxide, Sens. Actuators B 55 (1999) 154.
[27] P.P. Sahay, R.K. Nath, Al-doped zinc oxide thin films for liquid petroleum gas (LPG) sensors, Sens. Actuators B: Chem. 133 (2008) 222–227.
[28] A. Kolmakov, D.O. Klenov, Y. Lilach, S. Stemmer, M. Moskovits, Enhanced gas sensing by individual SnO_2 nanowires and nanobelts functionalized with Pd catalyst particle, Nano Lett. 5 (2005) 667–673.
[29] C.V. Gopal Reddy, S.V. Manorama, V.J. Rao, A. Lobo, S.K. Kulkarni, Noble metal additive modulation of gas sensitivity of $BaSnO_3$, explained by a work function based model, Thin Solid Films 348 (1999) 261.
[30] P. Montmeat, J.C. Marchand, R. Lalauze, J.P. Viricelle, G. Tournier, C. Pijolat, Physico-chemical contribution of gold metallic particles to the action of oxygen on tin dioxide sensors, Sens. Actuators B 95 (2003) 83.
[31] T.G. Nenov, S.P. Yordanov, Ceramic Sensors, Technology and Applications, Technomic Pub., Lancaster, 1996.